Computational Materials Science 100 (2015) 31–38

Contents lists available at ScienceDirect

Computational Materials Science

journal homepage: www.elsevier.com/locate/commatsci

A simulation-based determination of cap parameters of the modified Drucker–Prager cap model by considering specimen barreling during conventional triaxial testing

Hyunho Shin [a], Jong-Bong Kim [b], Seong-Jun Kim [c], Kyong Yop Rhee [d,*]

[a] Department of Materials Engineering, Gangneung-Wonju National University, 7 Jugheon-gil, Gangneung, Gangwon-do 210-702, Republic of Korea
[b] Department of Mechanical and Automotive Engineering, Seoul National University of Science and Technology, 232 Gongneung-ro, Nowon-gu, Seoul 139-743, Republic of Korea
[c] Department of Industrial, Information, and Management Engineering, Gangneung-Wonju National University, 150 Namwon-ro, Wonju, Gangwon-do 220-711, Republic of Korea
[d] Department of Mechanical Engineering, Kyunghee University, 1732 Dukyoungdae-ro, Yongin, Gyeonggi-do 446-701, Republic of Korea

ARTICLE INFO

Article history:
Received 28 August 2014
Received in revised form 10 October 2014
Accepted 13 October 2014
Available online 1 December 2014

Keywords:
Barreling
Conventional triaxial test
Modified Drucker–Prager cap model
Cap aspect ratio
Radius of the transition surface

ABSTRACT

Two types of cap parameters were determined by fitting the experimentally obtained triaxial deviator stress curves found in the literature using the modified Drucker–Prager cap model. The two types of parameters were extracted using the specimen model that deforms uniformly or non-uniformly (barreling). The parameter set extracted from the non-uniformly deforming specimen model reasonably predicted the experimental deviator stress curves obtained from the barreling specimen. However, when the parameter set extracted from the uniformly deforming specimen model was used to simulate the experimental curves from the barreling specimen, the prediction was inferior to the set from the non-uniformly deforming model. Considering versatile types and properties of particulate materials (e.g., ceramic, metal, pharmaceutical powders and soils), we suggest to verify the prediction capabilities of the parameter sets from each specimen model. The stress path of the barreling specimen during the conventional triaxial test was fairly complex depending on the position in the specimen. Pure hydrostatic loading was not achieved even during the hydrostatic loading stage. In the shear loading stage, the position-averaged stress path showed a lower slope in the meridional plane than that of the uniformly deforming specimen with a slope of $\sqrt{3}$.

1. Introduction

The computer simulation of the compaction behavior of particulate materials (e.g., ceramic, metal, pharmaceutical powders and soils) has received much interest [1–48]. In addition to the shear yielding (failure) behavior, particulate materials exhibit hydrostatic pressure-dependent yielding behavior, while the yielding of bulk metals do not exhibit the hydrostatic pressure dependency. In order to describe such yielding behavior of particulate materials, the modified Drucker–Prager cap (MDPC) constitutive model has been employed frequently in many engineering areas [2–46]. This model is suitable for a variety of application areas involving monotonic loading. The input information for the MDPC model includes parameters for describing elastic behavior, parameters that define the shear failure surface, parameters of the moving cap (the cap aspect ratio R and the transition surface radius α) that define the shape of the cap and transition yield surfaces, and the hydrostatic pressure vs. inelastic volumetric strain relation that govern the movement of the cap. Among the required input parameters, the cap parameters (i.e., R and α) are the most difficult to determine experimentally while its influence on the deformation behavior of the compacted particulate materials is higher than any of the other parameters [40,41].

In order to determine R and α experimentally, the conventional triaxial test [49] is generally used which measures the deviator stress curve as functions of axial and radial strain at varying confinement pressures. In an experimental approach, several series of isoplastic-volumetric-strain data points are displayed in the meridional plane [45–48], from which the R and α values are determined by a non-linear curve fitting. In this process, significant scattering of the iso-plastic-volumetric-strain data points is often found [45–48], which, along with the complexity of the method, may be a disadvantage of the experimental determination process. Because of the difficulty in determining the cap parameters experimentally, alternative methods have been developed. For instance,

* Corresponding author.
E-mail addresses: hshin@gwnu.ac.kr (H. Shin), jbkim@seoultech.ac.kr (J.-B. Kim), sjkim@gwnu.ac.kr (S.-J. Kim), rheeky@khu.ac.kr (K.Y. Rhee).

http://dx.doi.org/10.1016/j.commatsci.2014.10.024
0927-0256/

Wagle et al. [42] developed a numerical model to determine cap parameters from the measured distribution of the green density. Lu [43] developed a method that uses a combination of a numerical optimization method and material tests. An alternative method to simply determine the R and α values from conventional triaxial testing is to simulate the experimentally obtained triaxial deviator stress curve by assuming varying R [50,51] and α. The set of R and α, which simulates the triaxial curves most accurately at varying confinement pressures, is then selected. This approach may be called the simulation-based determination process, which is simpler and may result in a more reliable set of R and α values than the experimental approach.

In interpreting the triaxial deviator stress curve, it should not be overlooked that the triaxial specimen barrels significantly during the test of particulate materials: the specimen deforms non-uniformly. Although the non-uniform stress state in the barreled (non-uniformly deformed) specimen has been considered [52,53], there are few studies on the extent of curve (the true material properties) deviation under the influence of barreling. In this regard, we recently observed that there was a non-negligible influence of the specimen barreling on the determined deviator stress curve [54]; the triaxial curve was affected by both the true material properties and an artificial effect (i.e., specimen barreling). Therefore, any simulation of the triaxial behavior of the specimen needs to be carried out based on a specimen model that accounts for the barreling. However, most simulations reported in the literature were carried out using specimen models that deform uniformly [55,56]. If a simulated deviator stress curve for the model of the uniformly deforming (non-barreling) specimen reasonably fits the experimental curve obtained from the barreling specimen, the parameter set used for the simulation cannot be a true material parameter set. This is because, as mentioned above, the experimental curve is manifested not solely by the true material properties but includes the artificial effect of the non-uniform deformation (barreling) of the specimen. The parameter set used for the simulation can be regarded the true material parameter set only when the simulated triaxial deviator stress curve using the model of the barreling specimen reasonably fits the experimental curve.

Based on the above reasoning, it is of interest to investigate how much difference exists between the prediction capabilities of two types of the parameter sets determined under the assumptions of uniformly and non-uniformly deforming specimens. For this purpose, we numerically determined two types of the parameter sets for R and α, by fitting the experimentally determined triaxial deviator stress curves found in the literature [51]. Then, we compared the capability of two types of the parameter sets in predicting the experimental triaxial curve. We also investigated the stress path of the barreling specimen with reference to the uniformly deforming specimen. In this paper, positive sign is assigned to the compression.

2. Cap constitutive models

In order to describe the hydrostatic pressure-dependent yield phenomenon, Drucker and Prager [57] extended the von Mises yield criterion for metals by introducing a dependence on the hydrostatic pressure ($J_1/3$). The Drucker–Prager yield function is given by

$$f(J_1, J_{2D}) = \sqrt{J_{2D}} - \theta J_1 - k = 0 \tag{1}$$

where J_1 is the first stress invariant, J_{2D} is the second invariant of the deviatoric stress, and θ and k are positive material constants. When θ is zero, Eq. (1) reduces to the von Mises yield criterion. The parameters θ and k are related to the angle of internal friction and cohesion intercept, respectively, in the shear stress–normal stress domain on the failure surface.

In 1957, Drucker et al. [58] added a spherical cap to the Drucker–Prager failure criterion, which is known as the Drucker–Prager cap model. While the spherical yield surface cap that they proposed is one of the simplest yield surfaces to describe the concept of work hardening, the shape of the yield surface may not necessarily be circular. In this regard, an elliptical yield surface with varying aspect ratios was also considered [59,60]. The elliptical yield function is

$$f(J_1, J_{2D}, \varepsilon_v^p) = (J_1 - l)^2 + R^2 J_{2D} - (x(\varepsilon_v^p) - l)^2 = 0 \tag{2}$$

where R is the aspect ratio of the ellipse, l is the location of the intersection of the Drucker–Prager surface and the cap in the J_1 axis, and x is the position of the cap in the J_1 axis.

The yield criterion, which is composed of Eqs. (1) and (2), is implemented in a commercial finite element package, Abaqus [61], with the addition of a new yield surface (called the transition surface) located between the shear failure surface and the elliptical cap. This model is referred to as the modified Drucker-Prager cap (MDPC) model. The MDPC model is expressed in the $\sqrt{3J_{2D}} - p$ $(q - p)$ plane as seen in Fig. 1, instead of the $\sqrt{J_{2D}} - J_1$ plane. In the $q - p$ plane, the Drucker–Prager yield function (shear failure surface) is given by

$$f(p, q) = q - p\tan\beta - d = 0 \tag{3}$$

where d and β are defined in Fig. 1.

The transition surface is introduced for the purpose of the stability of the numerical analysis using the model. The radius of the transition surface is controlled by the parameter α as seen in the following equation [61]:

$$f(p, q, \varepsilon_v^p) = (p - p_a)^2 + [q - (1 - \alpha/\cos\beta)b]^2 - \alpha^2 b^2 = 0 \tag{4}$$

By the introduction of the transition surface to the MDPC model, the cap yield function of the MDPC model does not touch the shear failure surface as seen in Fig. 1. Thus, the cap yield function of the MDPC model is modified from Eq. (2) as follows [61].

$$f(p, q, \varepsilon_v^p) = (p - p_a)^2 + \left[\frac{Rq}{(1 + \alpha - \alpha/\cos\beta)}\right]^2 - R^2 b^2 = 0 \tag{5}$$

Since α controls not only the transition surface (Eq. (4)) but also the cap surface as seen in Eq. (5), α is called a cap parameter in this paper together with R that controls only the cap surface.

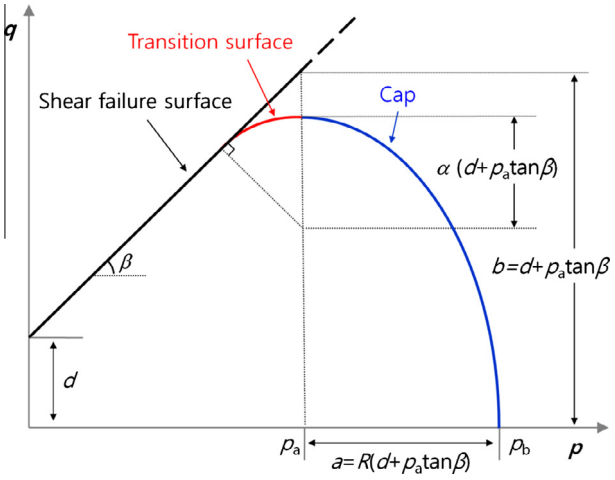

Fig. 1. Yield surfaces of the modified Drucker–Prager model in $\sqrt{3J_{2D}} - p$ $(q - p)$ plane [61].

In the numerical implementation of the MDPC model, the associated flow rule is applied on the cap surface while the non-associated flow rule is used for the transition surface and the shear failure surface [61]. As for the operation principle of the model, the cap represents a locus of points with the same volumetric inelastic strain and its position in the hydrostatic axis is controlled by the hydrostatic pressure vs. inelastic volumetric strain relation (hardening law). When the stress state reaches the cap, it expands to define a new yield surface according to the hardening law, which allows additional plastic deformation after the yielding of particulate materials (work hardening) prior to reaching the ultimate failure state defined by the failure surface. The moving cap also accounts for plastic deformation under pure hydrostatic loading. If a new stress state reaches the failure surface inside the cap by unloading, the cap contracts until the intersection point between the cap and the failure surface reaches the new stress state on the failure surface. Then, the position of p_b (defined in Fig. 1) decreases simultaneously, which represents the decrease of the inelastic volume strain (i.e., the dilation of the particulate materials) according to the hardening law.

3. Numerical experiment

Although one-quarter of the space of a cylindrical triaxial specimen can be analyzed by taking symmetry into account, the present investigation analyzes one-half of the 2D axisymmetric space (Fig. 2) to aid the visualization of the barreling phenomenon. The y-axis is the axis of symmetry. The modeled size of the radial x–y plane of the specimen was 0.75 in. (19.05 mm) in radius and 3.0 in. (76.20 mm) in height. The model was discretized using 4-node bilinear axi-symmetric quadrilateral elements. The number of elements for the specimen was 200 and the size of the elements passed a separate mesh quality test.

For the simulation of the uniformly deforming specimen, the nodes at the top of the specimen were allowed to move freely not only along the axial (y-axis) direction but also along the radial (x-axis) direction. The nodes at the bottom of the specimen were allowed to move only along the radial direction. For the non-uniformly deforming (barreling) specimen, an end constraint was imposed. The nodes at the top of the specimen were allowed to move only along the axial direction. The movement of nodes at the bottom of the specimen was fixed in all directions. For each type of specimens, the radial movement of the nodes along the y-axis was not allowed to reflect the axial symmetry.

In order to realize the hydrostatic loading condition, the same magnitude of the axial and radial pressure was applied to the top and radial (circumferential) surfaces of the model: the magnitude is the confinement pressure. For the subsequent deviatoric loading stage, the axial displacement of nodes at the top of the specimen was controlled (up to −20 mm which is 0.304 in axial strain) to achieve shear state of the specimen. The additional axial stress applied solely in the shear stage was determined by extracting the reaction force at the top end nodes and dividing it by the current area of the specimen. When simulating the uniformly deforming specimen, the current area was determined using information on the displacement of the node at the radial end of the specimen. When simulating the non-uniformly deforming specimen, the current area of the specimen was determined following the method that is utilized in a real experiment; the current area is calculated by assuming that the specimen remains as a right circular cylinder and by taking into account the volume change in the shear stage. Thus, the following equation was used [49]:

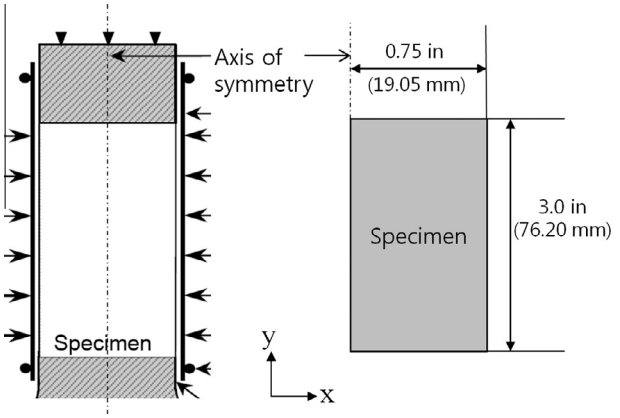

Fig. 2. Schematic illustration of the model for the finite element analysis.

$$A = \frac{A_o}{1-\varepsilon}\left(1+\frac{\Delta V}{V_o}\right) \tag{6}$$

where A is the cross sectional area of the specimen, A_o is the initial area at the beginning of the shear loading, ε is the axial strain (engineering) with reference to the initial length of the specimen at the beginning of the shear stage (positive for compression), and $\Delta V/V_o$ is the ratio of the volume change (ΔV) with reference to the initial volume (V_o) of the specimen at the beginning of the shear stage (positive for tension).

The parameter set of the MDPC model used in this study, which aims to simulate the triaxial deviator stress curve reported by Lee et al. [51], is summarized in Table 1. In order to obtain the failure surface parameters (i.e., d and β), the maximum (peak) deviator stresses of their triaxial curves at varying confinement pressures were transferred to the $\sqrt{J_{2D}} - p$ plane, and a linear fit was applied. The elastic parameters, i.e., the elastic modulus (E) and Poisson's ratio (ν), were adapted from their study [51]. The hardening law, i.e., the hydrostatic yield pressure (p) vs. inelastic volumetric strain (ε_v^{in}) relation, was obtained in this study by fitting their data set for the pressure-total volumetric strain (ε_v^{tot}) relation to a second order equation (as seen in Table 1); the elastic strain was assumed to be negligible in their (p, ε_v^{tot}) data set and their current volumetric strain was assumed to be the inelastic volumetric strain (the residual volumetric strain when unloaded). The cap parameters (R and α) were varied until they fit the experimental deviator stress vs. axial strain curves. In the Abaqus implementation of the MDPC model, the initial cap yield surface position on the hydrostatic pressure axis when the analysis begins is defined by the initial inelastic volume strain, $\varepsilon_v^{in}(0)$. As the initial cap position increases, the pressure required to plastically deform the material increases; the required pressure is determined by the hardening law. Thus, $\varepsilon_v^{in}(0)$ is the parameter that indicates the degree of initial compaction of the specimen. In this study, $\varepsilon_v^{in}(0)$ was set to zero for the simulation of the triaxial loading, which means that the required pressure to initiate the inelastic volume strain (plastic deformation) was set to be 47.381 kPa (see Table 1).

The MDPC model is described in the $q - p$ plane, where q is

$$q = \sqrt{3J_{2D}} = \sigma_a - \sigma_r \tag{7}$$

for the cylindrical specimen in the conventional triaxial test. Many researchers who investigated the behavior of particulate materials using the MDPC model described the yield criteria in the $\sqrt{J_{2D}} - p$ plane [2–6,46]. In this paper, we discuss the model parameters

Table 1
The parameter set of the MDPC model (in $\sqrt{J_{2D}} - p$ plane) used in this study. The cap parameters (R and α) were varied.

d (kPa)	β (°)	E (MPa)	ν	Hardening law (kPa) ($x = \varepsilon_v^{in}$)
27.095	41.117	80	0.35	$p = 783,694x^2 + 4,302.8x + 47.381$

(d, β, R) defined in the $\sqrt{J_{2D}} - p$ plane. Thus, for the numerical analysis using the MDPC model, some parameters were converted to those in the q-p space; both d and $\tan\beta$ were multiplied by $\sqrt{3}$ while R was multiplied by $1/\sqrt{3}$. α is the same for $\sqrt{J_{2D}} - p$ and $q - p$ planes.

4. Result and discussion

4.1. Determined parameter sets

The fitting process was carried out from the viewpoint of minimizing the deviation of the simulated curve from the experimental curve within the available range of the axial strain. Through the process described later in Section 4.2, a set of R and α values (0.7 and 0.01, respectively) was determined for the uniformly deforming specimen model and named parameter set A (Table 2). Fig. 3 shows the simulation result for the uniformly deforming specimen model when parameter set A was used. This parameter set (A) reasonably fits the maximum deviator stress at varying confinement pressures for the uniformly deforming specimen model. The deformed shapes of the specimen were right circular cylinders and the stress state within the specimen was uniform (not shown).

Using the process described later in Section 4.2, we also determined a set of R and α values (0.7 and 0.03, respectively) for the non-uniformly deforming (barreling) specimen model and named parameter set B (Table 2). As seen in Fig. 4, this parameter set (B) also fits the triaxial deviator stress curves acceptably for the non-uniformly deforming specimen model at varying confinement pressures.

The deformed shape of the specimen predicted by the parameter set B for the non-uniformly deforming specimen model is shown in Fig. 5 when the axial strain is 9% and the confinement pressure is 103 kPa (the positions marked as 1, 2, and 3 are explained later in Fig. 9). In Fig. 5, both the axial and radial stresses are non uniform within the specimen which explains the non-uniformly deformed (barreled) shape.

4.2. Effects of R and α on the deviator stress curve

This subsection presents the result of the parametric study for R and α. As seen in Fig. 6(a) for the uniformly deforming specimen model, the decrease of R from 0.7 to 0.55 shifted the simulated curves mainly to the left side (or right side for an increased R) in the axial strain axis. The change in R did not result in a change in the ultimate deviator stress level when the axial stress was sufficiently large: the value of R influenced only the rising part of the deviator stress curve. The increase of α from 0 to 0.1 shifted the simulated curves (ultimate q value when the axial strain is sufficiently large) mainly downward (or upward for a decreased α). For the non-uniformly deforming specimen model (Fig. 6(b)), the influences of R and α were similar to those in the uniformly deforming specimen model while the influence of α at a given confinement pressure was diminished in the non-uniformly deforming model.

The findings of the shift directions of the simulated curves depending on R at a given α (or depending on α at a given R) reduced the number of trials greatly. Once these shift directions are noted, the best value of each parameter can be found with only at a few trials for the barreling or non barreling specimen model.

Table 2
Determined sets of the cap parameters (R and α).

Notation of the parameter set	R	α	Used specimen model to determine the parameter set
A	0.7	0.01	Uniformly deforming specimen model
B	0.7	0.03	Non-uniformly deforming specimen model

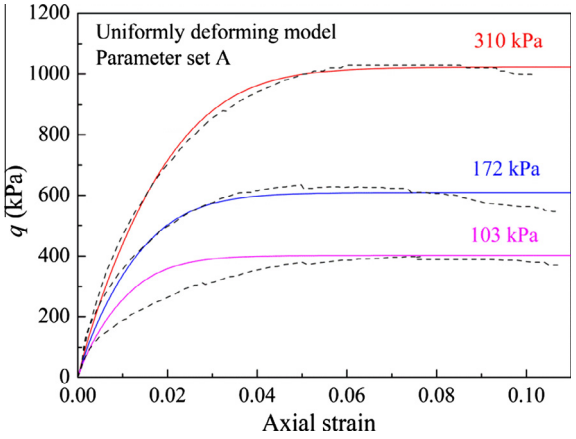

Fig. 3. Simulated curves (solid) for the uniformly deforming specimen model using parameter set A (R = 0.7, α = 0.01) and experimental curves (dashed [51]).

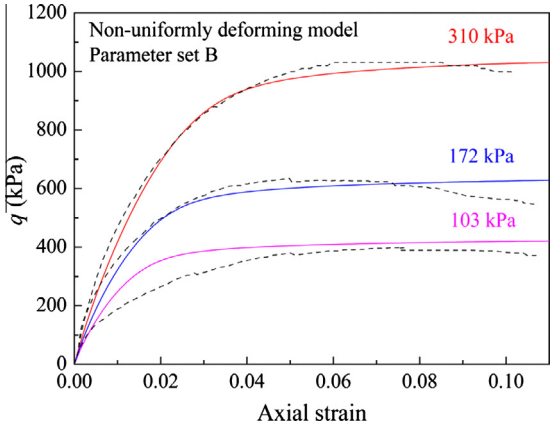

Fig. 4. Simulated curves (solid) for the non-uniformly deforming specimen model using parameter set B (R = 0.7, α = 0.03) and experimental curves (dashed [51]).

The parameters sets A and B have the same value of R (Table 2), which means that the consideration of the specimen barreling did not result in the change in R in the simulation cases. This finding results from the fact that the specimen barreling is not significant in the early period of the shear loading stage (in the rising part of the deviator stress curve). However, the barreling of the specimen resulted in a different value of α from that of the uniformly deforming specimen (Table 2).

In the experimental deviator stress curves (Fig. 4), the peak stress appears at an axial strain (ε_a) value of approximately 0.050–0.075 depending on the confinement pressures. As seen in Fig. 6(a), when the uniformly deforming model is used, the MDPC model is incapable of predicting the peak stress in the loading curve. When the non-uniformly deforming model is used (Fig. 6(b)), the peak stress is predicted only when the axial strain is fairly large (at a ε_a value of approximately 0.15) and the confinement pressure is high (310 kPa); this phenomenon results from the specimen barreling. Although the experimental peak stress at a small ε_a of approximately 0.050–0.075 may partly be due to the specimen barreling, it is most likely mainly the result of the nature of the specimen (e.g., over-consolidated specimen [44,49,69]) because the phenomenon of barreling is not significant at such a small strain. In order to predict the peak stress at small axial

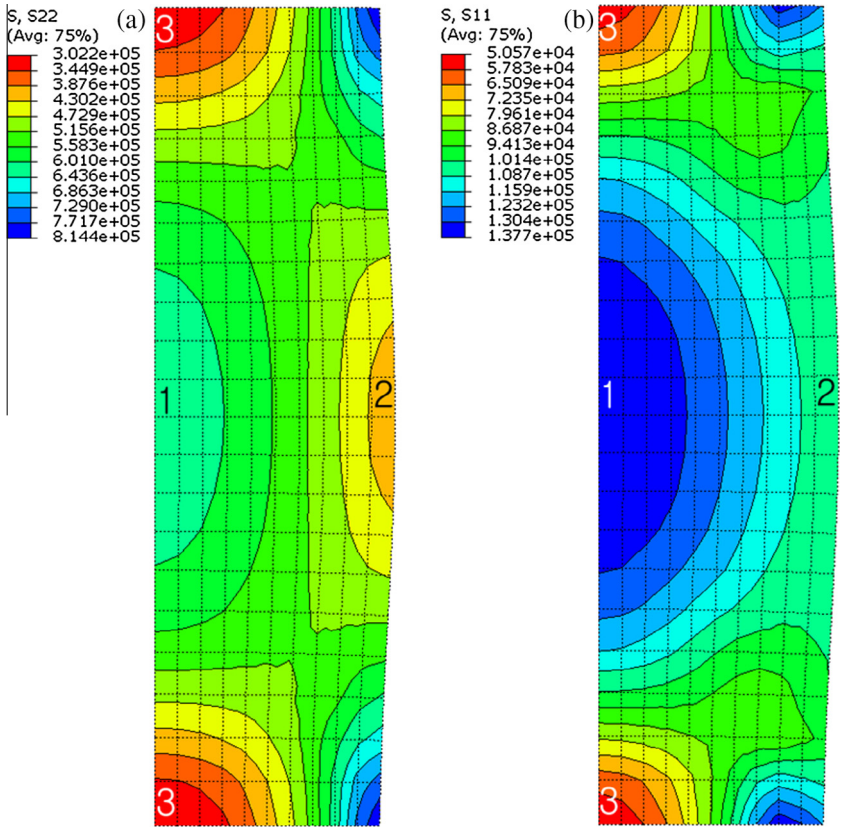

Fig. 5. (a) Axial and (b) radial stress contours of the deformed specimen when the axial strain is 0.09 and the confinement pressure is 103 kPa. Parameter set *B* ($R = 0.7$, $\alpha = 0.03$) was used.

strains (the nature of the specimen) where the influence of the barreling is insignificant, a more sophisticated constitutive model with more parameters, such as the single hardening constitutive model [44,62–64], may be needed.

4.3. Importance of considering the specimen barreling

Comparing Fig. 3 (parameter set *A*) with Fig. 4 (parameter set *B*), it appears that parameter set *A* similarly predicts the experimental curves to the set *B*. However, note that the simulated curves in Fig. 3 were for the uniformly deforming model. If a given parameter set is a true material property, it should reasonably describe any loading event if the event belongs to the target area for which the model was developed. It is assumed that the determination process of the two parameter sets is unknown (i.e., they were simply received from elsewhere). The capability of the parameter sets (*A* and *B*) can be tested if triaxial testing is simulated and compared with the experimental result. Because the barreling occurred during the experiment [51] that is considered in this study, it is natural to use a specimen model that considers barreling. Therefore, we applied parameter set *A* to the non-uniformly deforming (barreling) model and show the resultant simulation curves in Fig. 7 (the case when parameter set *B* is applied to the non-uniformly deforming model is already shown in Fig. 4). The use of parameter set *A* in the non-uniformly deforming model also resulted in barreling (not shown) that was very similar to the deformed shape shown in Fig. 5.

For the comparison of the prediction capabilities of parameter sets *A* and *B* in the non-uniformly deforming specimen model (Figs. 7 and 4, respectively), the mean absolute deviation (D_m) and fitting errors [65] were quantified by the relations,

$$D_m = \frac{\sum |q_{\text{sim}} - q_{\text{exp}}|}{n} = \frac{\int_0^{\varepsilon^{\text{m}}} |q_{\text{sim}} - q_{\text{exp}}| d\varepsilon}{\varepsilon^{\text{m}}} \tag{8}$$

and

$$\text{Error}(\%) = \frac{\int_0^{\varepsilon^{m}} |q_{\text{sim}} - q_{\text{exp}}| d\varepsilon}{\int_0^{\varepsilon^{\text{m}}} q_{\text{exp}} d\varepsilon} \times 100 \tag{9}$$

where n is the number of data points, q_{exp} and q_{sim} are experimental and simulated deviator stresses, respectively, ε is the axial strain, and ε^{m} is the maximum axial strain of the experiment. The calculated results are summarized in Table 3 for parameter sets *A* and *B*.

From Table 3, parameter set *B* is a better choice as it shows an improved result. Thus, it is desirable to include the barreling specimen model in the simulation-based determination process of the cap parameters, in addition to the conventionally investigated specimen model of the uniform deformation. Since there are versatile types and properties of particulate materials (e.g., ceramic, metal, pharmaceutical powders, and soils), the prediction capabilities of the two types of the parameter sets should be examined before applying the parameter set to versatile particulate materials. This suggestion may be applied to cases where other types of the cap models, such as the geologic cap model [66,67] and the continuous surface cap model [66,68], are used to determine the cap parameters.

This study fitted the experimental curves with the non-zero value of α purely from the viewpoint of minimizing the deviation of the simulated curve from the experiment in order to investigate the necessity of considering the non-uniformly deforming specimen model. From the notion that α was introduced to the MDPC model to ensure the stability in the numerical implementation of the model (α is not a material constant), we separately determined

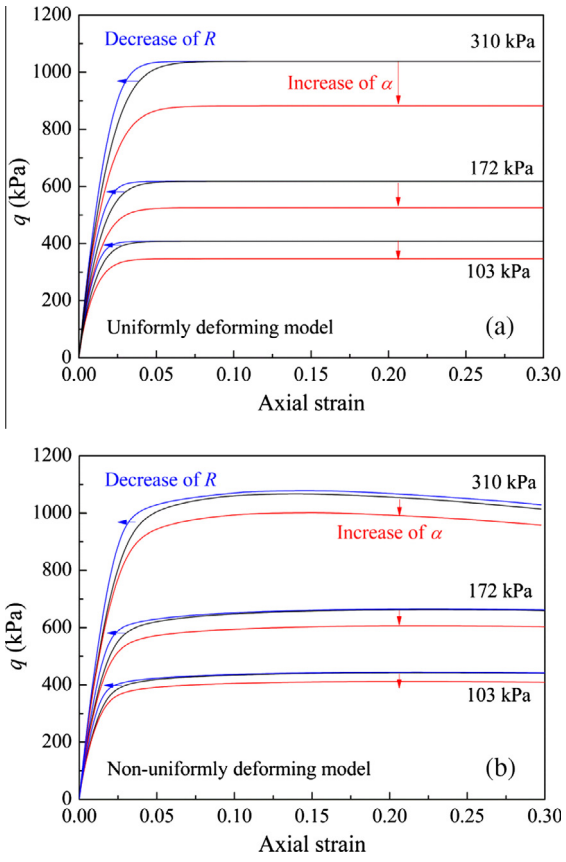

Fig. 6. Simulation results for the (a) uniformly and (b) non-uniformly deforming specimen models. The black curves are for the (R, α) set of (0.7, 0). The blue curves are when R decreases from 0.7 to 0.55 and the red curves are when α increases from 0 to 0.1. (For interpretation of the references to colour in this figure legend, the reader is referred to the web version of this article.)

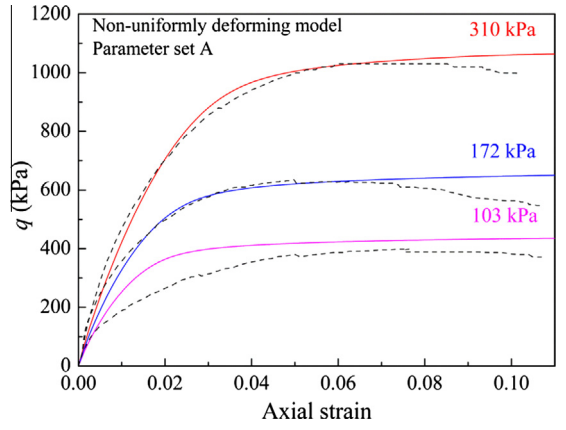

Fig. 7. Simulated curves (solid) for the non-uniformly deforming specimen model using parameter set A ($R = 0.7$, $\alpha = 0.01$) and experimental curves (dashed [51]).

Table 3
Mean absolute deviation and fitting errors of the simulated curves for parameter sets A and B in the non-uniformly deforming specimen model.

Quantification tool	Mean absolute deviation (kPa)		Fitting error (%)	
	Set A	Set B	Set A	Set B
Curve at 103 kPa	52.65	40.56	15.85	12.21
Curve at 172 kPa	12.59	4.37	2.30	0.80
Curve at 310 kPa	19.81	5.24	2.29	0.61

the R value by setting the value of α as zero for the non-uniformly deforming specimen model. The result is shown in Supplementary Material (Fig. S1). The prediction in this way (Table S1; parameter set C) is inferior to parameter set B shown in Table 3 (this result arises from the limitation of the MDPC model, which cannot describe the specimen-nature-induced peak stress in the deviator stress curve). In the experimental determination, however, R needs to be determined by setting α as zero because α is not a material property. The user of the model may set a non-zero value of α from the viewpoint of apparently fitting an engineering event. If the engineering event of interest is simulated successfully with only an overly large α, it results from the numerical fiction of the model (the limitation of the model) because α is not a material constant.

4.4. Stress path of the barreling specimen

In this subsection, we compare the stress path of the barreling specimen with the uniformly deforming (non-barreling) specimen. For this purpose, $\sqrt{J_{2D}}$ and p were calculated by averaging the stresses (σ_a and σ_r) of all of the specimen elements. Parameter set B was used for the uniformly and non-uniformly deforming specimen models, respectively. Fig. 8 shows the simulated stress path in the $\sqrt{J_{2D}} - p$ plane. In the hydrostatic loading stage, the uniformly deforming specimen follows the abscissa (the horizontal line at $\sqrt{J_{2D}} = 0$) regardless of the confinement pressure; a pure hydrostatic pressure is applied to the specimen. During the deviatoric loading stage, the slope of the stress path is $\sqrt{3}$ for the uniformly deforming specimen regardless of the confinement pressures, which is consistent with the theoretical slope of the stress path in the conventional triaxial test [69].

Pure hydrostatic loading is not achieved in the non-uniformly deforming specimen. As seen in Fig. 8, the loading path shifts from the abscissa during the hydrostatic loading stage and thus a deviatoric stress component is included. Subsequently, the applied hydrostatic pressure (i.e., 103, 172, and 310 kPa) is not delivered properly to the specimen so a lower magnitude of pressure (96.9, 161.7, and 292.3 kPa, respectively) is applied to the specimen at the end of the hydrostatic loading stage. The higher the confinement pressure, the higher the deviation from the pure hydrostatic loading. This finding indicates that a correction is needed when experimentally constructing the $p - \varepsilon_v^{in}$ relation using the conventional triaxial test especially in a high pressure regime. The slope of the stress path in the shear loading stage is smaller than $\sqrt{3}$, and the stress path changes its slope when the stress state is near the failure surface. Such deviations from the load path of the uniformly deforming specimen result from the end constraint of the

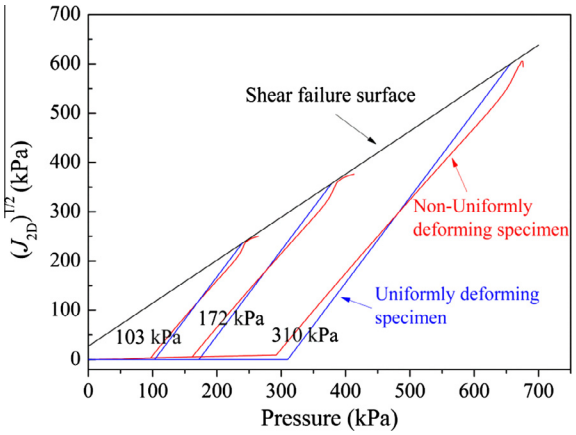

Fig. 8. Stress paths in $\sqrt{J_{2D}} - p$ plane for the uniformly deforming (blue) and the non-uniformly deforming specimens (red). (For interpretation of the references to colour in this figure legend, the reader is referred to the web version of this article.)

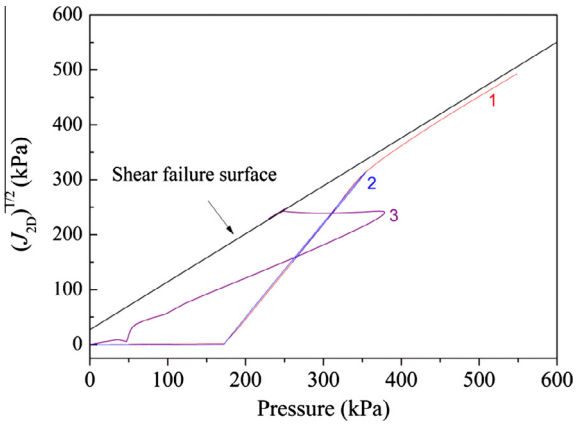

Fig. 9. Stress paths of the three selected elements (positions) marked in Fig. 5. The confinement pressure was 172 kPa. The color of the position number is matched to that of the curve.

specimen which is applied to the top and bottom support; the end restraint limits the radial contraction of such portions in the specimen.

Because the stress path of the non-uniformly deforming specimen was constructed in Fig. 8 using the average stresses (σ_a and σ_r) of all the elements in the specimen (the stress state of the uniformly deforming specimen is the same regardless of the element position), we selected three elements located at different positions (marked in Fig. 5), and illustrate the stress path of the selected locations in Fig. 9.

As seen in Fig. 9, the stress path of the non-uniformly deforming specimen is fairly complex depending on the specimen position. Position number 1 (the center of the specimen) deviates only slightly from the stress path of the uniformly deforming specimen. At the end of the deviatoric loading stage, the load path approaches the failure surface asymptotically but never reaches the failure surface up to the at the axial strain of 0.304. Position number 2 (barreled portion of the specimen) follows a similar load path to position number 1. However, when the stress state is near the failure surface, the load path reverses its direction and retraces the loading path toward the initial state of the shear loading stage. Position number 3 (the center of the top and bottom planes in the specimen) shows the most significant deviation from the load path of the uniformly deforming specimen. The load path deviates significantly even during the hydrostatic loading stage and finally reaches the failure surface.

5. Conclusion

The cap parameters (the cap aspect ratio and the transition surface parameter) of a cap constitutive model can be reliably determined by simulating the deviator stress curves of the conventional triaxial test for particulate materials using varying sets of the cap parameters until they reasonably fit the experimental curves. In this study, two types of cap parameters were determined by fitting the experimentally obtained triaxial deviator stress curves found in the literature using the modified Drucker–Prager cap model. The two types of the parameters were extracted from the specimen model that deforms uniformly or non-uniformly (barreling). The parameter set from the non-uniformly deforming specimen model (set *B*) reasonably predicted the experimental deviator stress curves obtained from the barreling specimen. However, when the parameter set from the uniformly deforming specimen model (set *A*) was used to simulate the experimentally obtained triaxial curves from the barreling specimen, the prediction was inferior to parameter set *B*. Considering versatile types and properties of particulate materials (e.g., ceramic, metal, pharmaceutical powders and soils), we suggest to include the barreling specimen model in the simulation-based determination process of the cap parameters, in addition to the conventionally investigated specimen model of the uniform deformation, and verify the capabilities of the parameter sets determined from each model. For the barreling specimen, pure hydrostatic loading was not achieved even during the hydrostatic loading stage, and thus a correction is needed when experimentally constructing the $p - \varepsilon_v^{\text{in}}$ relation using the conventional triaxial test especially in a high pressure regime. The stress path of the barreling specimen was fairly complex depending on the position in the specimen even during the hydrostatic loading stage. In the shear loading stage, the position-averaged stress path showed a lower slope in the meridional plane than that of the uniformly deforming specimen with a slope of $\sqrt{3}$.

Acknowledgments

The first author (H. Shin) appreciates the technical assistance of Ms. Eun-Hee Jung at the Industry-Academy Cooperation Foundation of Gangneung-Wonju National University, Republic of Korea. This work was supported by the Basic Science Research Program through the National Research Foundation of Korea (NRF) funded by the Ministry of Education, Science and Technology (Project number: 2013R1A1A2A10063466).

Appendix A. Supplementary material

Supplementary data associated with this article can be found, in the online version, at http://dx.doi.org/10.1016/j.commatsci.2014.10.024.

References

[1] I. Aydin, B.J. Briscoe, K.Y. Şanhtürk, Comput. Mater. Sci. 3 (1994) 55–68.
[2] I. Aydin, B.J. Briscoe, K.Y. Şanhtürk, Powder Technol. 89 (1996) 239–254.
[3] I. Aydin, B.J. Briscoe, K.Y. Şanhtürk, J. Eur. Ceram. Soc. 17 (1997) 1201–1212.
[4] A. Michrafy, D. Ringenbacher, P. Tchoreloff, Powder Technol. 127 (2002) 257–266.
[5] C.-Y. Wu, O.M. Ruddy, A.C. Bentham, B.C. Hancock, S.M. Best, J.A. Elliott, Powder Technol. 152 (2005) 107–117.
[6] C.-Y. Wu, B.C. Hancock, A. Mills, A.C. Bentham, S.M. Best, J.A. Elliott, Powder Technol. 181 (2008) 121–129.
[7] L.H. Han, J.A. Elliott, A.C. Bentham, A. Mills, G.E. Amidon, B.C. Hancock, Int. J. Solids Struct. 45 (2008) 3088–3106.
[8] L.H. Han, J. Elliott, S. Best, R. Cameron, A.C. Bentham, A. Mills, G.E. Amidon, B.C. Hancock, Mater. Sci. Forum 575–578 (2008) 560–565.
[9] L.H. Han, P.R. Laity, R.E. Cameron, J.A. Elliott, J. Mater. Sci. 46 (2011) 5977–5990.
[10] I.C. Sinka, J.C. Cunningham, A. Zavaliangos, J. Pharm. Sci. 93 (8) (2004) 2040–2052.
[11] J.C. Cunningham, I.C. Sinka, A. Zavaliangos, J. Pharm. Sci. 93 (8) (2004) 2022–2039.
[12] I.C. Sinka, KONA 25 (2007) 4–22.
[13] I.C. Sinka, J.C. Cunningham, A. Zavaliangos, Powder Technol. 133 (2003) 33–44.
[14] C. Shang, I.C. Sinka, J. Pan, Exp. Mech. 52 (2012) 903–916.
[15] H. Zipse, J. Eur. Ceram. Soc. 17 (1997) 1707–1713.
[16] P. Chen, G.Y. Kim, J. Ni, J. Mater. Proc. Technol. 190 (2007) 243–250.
[17] W. Chen, Y. Yamamoto, W.H. Peter, S.B. Gorti, A.S. Sabau, M.B. Clark, S.D. Nunn, J.O. Kiggans, C.A. Blue, J.C. Williams, B. Fuller, K. Akhtar, Powder Technol. 214 (2011) 194–199.
[18] O.G. Abdullah, F.A. Rasin, T.A. Al-Dhahir, J. KUFA-Phys. 1 (2009) 12–24.
[19] O.G. Abdullah, F.A. Rasin, T.A. Al-Dhahir, Int. J. Pure Appl. Phys. 5 (2009) 15–31.
[20] R.Z. Moayed, S. Tamassoki, E. Izadi, World Acad. Sci. Eng. Technol. 6 (2012) 939–943.
[21] R. Zhou, L.-H. Zhang, B.-Y. He, Y.-H. Liu, Trans. Nonferrous Met. Soc. China 23 (2013) 2374–2382.
[22] G. Si, L. Chen, H. Shi, Y. Xie, R. Heng, Chin. J. Pharm. 44 (2013) 88–94.
[23] G.N. Si, L. Chen, Appl. Mech. Mater. 217–219 (2012) 2117–2120.
[24] Y.Y. Foo, Y. Sheng, B.J. Briscoe, Int. J. Solids Struct. 41 (2004) 5929–5943.
[25] Y.-B. Kim, J. Lee, S. Lee, H.-J. Park, G.-A. Lee, Adv. Mater. Res. 482–484 (2012) 1249–1256.

[26] T. Sinha, J.S. Curtis, B.C. Hancok, C. Wassgren, Powder Technol. 198 (2010) 315–324.
[27] T. Sinha, R. Bharadwaj, J.S. Curtis, B.C. Hancok, C. Wassgren, Powder Technol. 202 (2010) 46–54.
[28] O. Coube, H. Riedel, Powder Metall. 43 (2000) 123–131.
[29] T. Kraft, H. Riedel, O. Rosenfelder, Int. J. Powder Metall. 39 (2003) 27–34.
[30] T. Kraft, Modell. Simul. Mater. Sci. Eng. 11 (2003) 381–400.
[31] T. Kraft, H. Riedel, P. Stingl, F. Wittig, Adv. Eng. Mater. 1 (1999) 107–109.
[32] J.-D. Prigge, K. Sommer, Particulate Sci. Technol. 29 (2011) 40–52.
[33] D. Volik, Int. J. GEOMATE 1 (2011) 135–139.
[34] M.Y. Fattah, M.J. Al-Mosawi, A.A.O. Al-Zayadi, Geomech. Eng. 5 (2013) 17–36.
[35] A. Azimi, J. Kövecses, J. Angeles, IEEE Trans. Robotics 29 (2013) 1271–1288.
[36] B.M. Luccioni, M. Luege, Int. J. Impact Eng. 32 (2006) 1248–1266.
[37] E. Stilger-Szydło, W. Tutaj, Studia Geotech. Mech. 26 (2004) 3–22.
[38] R.C. Chiroux, W.A. Foster Jr., C.E. Johnson, S.A. Shoop, R.L. Raper, Appl. Math. Comput. 162 (2005) 707–722.
[39] I.-H. Ho, C.-C. Hsieh, J. GeoEng. 8 (3) (2013) 91–100.
[40] Y. He, R.S. Engel, N.J. Salamon, R. Zhang, Sensitivity study and parameter determination for 316l stainless steel powder die compaction, in: Proc. 2002 International Conference on Process Modeling in Powder Metallurgy (Process Modeling in Powder Metallurgy & Particulate Materials), 2002, pp. 99–106.
[41] G.S. Wagle, R.S. Engel, R. Bollina, R.M. German, Statistical analysis of modified Drucker–Prager cap model parameters for applications to modeling die compaction, in: Proceedings of the 2003 International Conference on Powder Metallurgy & Particulate Materials, Part IV, 2003, pp. 24–36.
[42] G. Waggle, Die Compaction Simulation: Simplifying the Application of a Complex Constitutive Model Using Numerical and Physical Experiments, Ph.D. Thesis, The Pennsylvania State University, 2006.
[43] C. Lu, Determination of Cap Model Parameters using Numerical Optimization Method for Powder Compaction, Ph.D. Thesis, Marquette University, 2009.
[44] S. Helwany, Applied Soil Mechanics with ABAQUS Applications, vol. 34, John Wiley and Sons, Inc., Hoboken, 2007. pp. 34, 61–67, 68–86.
[45] K.T. Kim, S.W. Choi, H. Park, Trans. ASME 122 (2000) 238–244.
[46] D.H. Zeuch, J.M. Grazier, J.G. Argüello, K.G. Ewsuk, J. Mater. Sci. 36 (2001) 2911–2924.
[47] S.C. Lee, K.T. Kim, Int. J. Mech. Sci. 44 (2002) 1295–1308.
[48] H.G. Kim, O. Gillia, P. Dorémus, D. Bouvard, Int. J. Mech. Sci. 44 (2002) 2523–2539.
[49] J.P. Bardet, Experimental Soil Mechanics, Prentice Hall, Upper Saddle River (NJ), 1997, pp. 370–374, 443–469.
[50] A.F. Fossum, P.E. Senseny, T.W. Pfeifle, K.D. Mellegard, Mech. Mater. 21 (1995) 119–137.
[51] K.Z.Z. Lee, N.-Y. Chang, K.T. Chang, Determination of cap model parameters using drained conventional triaxial compression test results, in: Modernization and Optimization of Existing Dams and Reservoirs, (27th Annual USSD Conference, Philadelphia, Pennsylvania, March 5–9, 2007; U.S. Army Corps of Engineers), 2007, pp. 275–284.
[52] D. Sheng, B. Westerberg, H. Mattson, K. Axelsson, Comput. Geotech. 21 (3) (1997) 163–182.
[53] Q. Yang, J. Ge, Electronic J. Geotech. Eng. 17 (2012) 699–707.
[54] H. Shin, J.-B. Kim, Y.-H. Yoo, D.-B. Jeong, A numerical study on the effect of end restraint of specimen in conventional triaxial test on the yield strength and post-yield behavior of soil, The Collection of Scientific Papers. Series: Machinery and Building Constructions, third ed., Part I. 8th Ukrainian Conference Geotechnics and Foundations, vol. 38, Poltava National Technical Yuri Kondratyuk University, Poltava, 2013, pp. 29–36.
[55] S. Dolarevic, A. Ibrahimbegovic, Comput. Struct. 85 (2007) 419–430.
[56] R. Kohler, G. Hofstetter, Int. J. Numer. Anal. Meth. Geomech. 32 (2008) 981-104.
[57] D.C. Drucker, W. Prager, Q. Appl. Math. 10 (1952) 157–165.
[58] D.C. Drucker, R.E. Gibson, D.J. Henkel, Trans. Am. Soc. Civil Eng. 112 (1957) 338–346.
[59] F.L. DiMaggio, I.S. Sandler, J. Eng. Mech. Div. ASCE 97 (EM3) (1971) 935–950.
[60] I.S. Sandler, D. Rubin, J. Numer. Anal. Meth. Geomech. 3 (1979) 173–186.
[61] Dassault Systèmes Simulia Corp., ABAQUS Theory Manual 6.13, 2013.
[62] K.T. Kim, P.V. Lade, Comput. Geotech. 5 (1988) 307–324.
[63] P.V. Lade, K.T. Kim, Comput. Geotech. 6 (1988) 13–29.
[64] P.V. Lade, K.T. Kim, Comput. Geotech. 5 (1988) 31–47.
[65] J.B. Kim, H. Shin, Int. J. Impact. Eng. 36 (2009) 746–753.
[66] Livermore Software Technology Corp., LS-DYNA Keyword User's Manual, vol. II, Material Models, 2012.
[67] A.R. Khoei, S.O.R. Biabanaki, A.R. Vafa, S.M. Taheri-Mousavi, Comput. Mater. Sci. 46 (2009) 203–229.
[68] L.E. Schwer, Y.D. Murray, Continuous surface cap model for geomaterial modeling: a new LS-DYNA material type, in: 7th Int. LS-DYNA User's Conference, 2009, pp. 16–35–16–50.
[69] W.-F. Chen, Constitutive Equations for Engineering Materials, vol. 2, Elsevier, New York, 1994. pp. 1004–1008, 1013–1014.

Supplementary Material

A simulation-based determination of cap parameters of the modified Drucker-Prager cap model by considering specimen barreling during conventional triaxial testing

Hyunho Shin, Jong-Bong Kim, Sung-Jun Kim, Kyong Yop Rhee

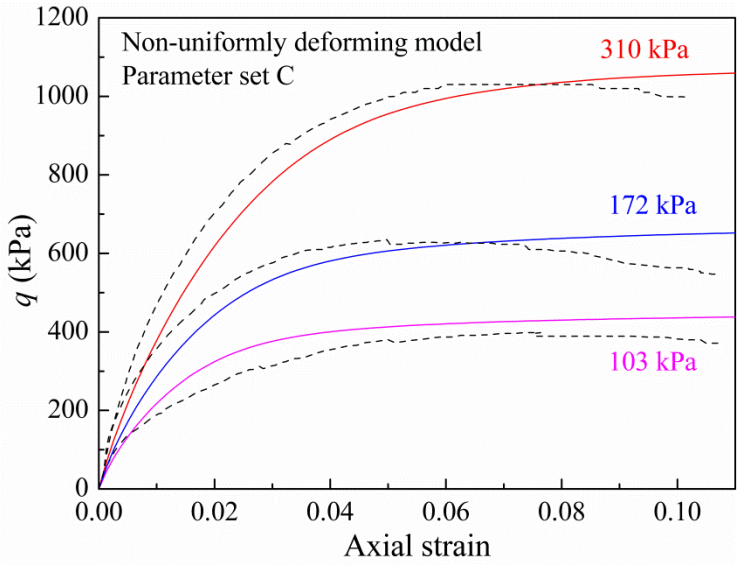

Fig. S1. Simulated curves (solid) for the non-uniformly deforming specimen model using the parameter set of R=0.92 and α=0 (named parameter set C in this Supplementary Material) and experimental curves (dashed [51]).

Table S1. Mean absolute deviation and fitting errors of the simulated curves for parameter set C (R=0.92, α=0) in the non-uniformly deforming specimen model.

Quantification tool	Mean absolute deviation (kPa)	Fitting error (%)
Curve at 103 kPa	41.66	12.54
Curve at 172 kPa	7.08	1.30
Curve at 310 kPa	22.95	2.65